Long-Term Datasets for the Understanding of Solar and Stellar Magnetic Cycles
Proceedings IAU Symposium No. 340, 2018
D. Banerjee, J. Jiang, K. Kusano & S. Solanki, eds.

doi:10.1017/S1743921318001023

Coronal magnetic field measurements using forbidden emission lines

A. Megha[1], M. Sampoorna[1], K. N. Nagendra[1] and K. Sankarasubramanian[1,2,3]

[1]Indian Institute of Astrophysics, Bengaluru, India ; email: megha@iiap.res.in

[2]ISRO Satellite Centre, Bengaluru, India ; [3] CESSI, IISER, Kolkata, India

Abstract. The polarization measurement of coronal forbidden emission lines is the most promising method of determining the direction of magnetic fields in the corona. A classical theory for the forbidden lines was presented in Megha *et al.* (2017) for the case of arbitrary strength magnetic fields. Here we apply that theoretical formalism to study the effect of density distributions, magnetic field configurations, and velocity fields on the Stokes profiles formed in corona. For illustrations we use the atomic parameters of the [Fe XIII] 10747 Å coronal forbidden line.

Keywords. Sun: corona - Sun: magnetic fields - line: profiles - polarization

1. Introduction

Coronal forbidden emission lines are formed due to the magnetic dipole (M1) transitions in highly ionized atoms in the solar corona. Polarization in these lines arises from anisotropic excitation of ions in the corona. Megha *et al.* (2017) used the M1 classical oscillator model of Casini & Lin (2002) and calculated the scattering matrix following Stenflo (1994). We considered a two-level atom ($J = 0 \rightarrow 1 \rightarrow 0$ transition) in arbitrary field strengths and neglected collisional effects. Scattering matrix so derived covers the field strength regime of Hanle, saturated Hanle, Hanle-Zeeman, and pure Zeeman effects.

2. Model parameters

We consider scattering on [Fe XIII] 10747 Å line with Einstein's A coefficient = 14.04 $\sec^{-1}$. For T = 2 MK, Doppler width of this line is 0.87 Å. We consider radial and dipole field configurations with average coronal field strength of 10 G. We consider two types of density distributions namely, spherically symmetric density (SSD) model of House (1972): $N_e(r) = \sum_{i=1}^{3} k_i\,(1+\rho)^{-\beta_i}$, and latitude ($\lambda$) dependent density (LDD) model of Saito (1970) for sunspot minimum: $N_e(r,\lambda) = 10^8 \times \{3.09(1-0.5\sin\lambda)(1+\rho)^{-16} + 1.58(1-0.95\sin\lambda)(1+\rho)^{-6} + 0.025(1-\sqrt{\sin\lambda})(1+\rho)^{-2.5}\}$, where $\rho = r/R_\odot$.

3. Maps of degree of linear polarization and position angle

For the model given in Section 2, we calculate the line-of-sight (LOS) integrated degree of linear polarization P= $\sqrt{Q^2+U^2}/I$ and position angle PA = $0.5\tan^{-1}(U/Q)$ as described in Megha *et al.* (2017). Figure 1 shows the map of P and PA for SSD and LDD. For radial field with SSD, P increases with height and reaches a maximum of 73.3%. Here PA lies along the radius vector. Unlike the SSD case, the map of P for LDD is asymmetric and reaches a maximum of 73.29 % in the polar region. However PA continues to be along the radius vector. For the dipole field the Van Vleck effect is seen wherein P is identically zero (symmetric black regions in map) when $\vartheta_B = \vartheta_V = 54.7^\circ$ (namely, $\lambda = 19.5^\circ$ and ϑ_V =Van Vleck angle). The PA follows the field lines for $\vartheta_B < \vartheta_V$ and becomes perpendicular to field lines for $\vartheta_B > \vartheta_V$ (radial). For a given radius, P is maximum near the

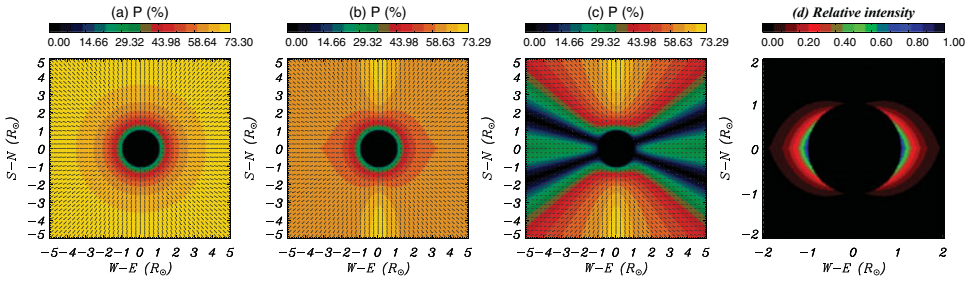

Figure 1. Maps of linear polarization. Short bars represent the PA. *a*, *b*, and *c* correspond respectively to radial field with SSD and LDD, and dipole field with LDD. *d* shows the relative intensity for LDD, which is proportional to the density distribution in corona.

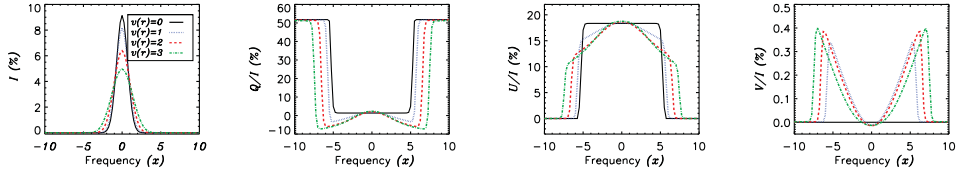

Figure 2. Stokes profiles v/s frequency $x = (\nu - \nu_0)/\Delta\nu_D$ for $r = 1.5R_\odot$, for radial velocity fields $v(r) = 0, 1, 2, 3$. The results are shown at co-latitude 60° in a dipole field.

poles and uniformly decreases until the Van Vleck region and then increases marginally until the equator, showing a symmetry about N-S and E-W directions.

4. Effect of a constant radial velocity field $v(r)$ on Stokes profiles

Figure 2 shows LOS integrated Stokes profiles for different $v(r)$. These profiles exhibit broadening that increases with $v(r)$. This is because for $-\pi/2 \leqslant \chi < 0$ (see Figure 6 of Megha *et al.* (2017) for χ definition) the profiles are red shifted and for $0 < \chi \leqslant \pi/2$ the profiles are blue shifted. Q/I and U/I show significant changes in the line core. $V/I = 0$ in the static case (due to opposite signs of V/I in forward and backward lobes with respect to midplane $\chi = 0°$). In the presence of velocity fields V/I exhibit a non-zero double-peaked shape. These changes are due to combined effects of spherical geometry (radius vector making smaller and smaller angles with respect to LOS, as we move away from the midplane) and the projected velocity field.

5. Conclusions

For the chosen density distribution, the intensity is more sensitive to the density gradient than P for $1 \lesssim R < 2R_\odot$. For $R \gtrsim 2R_\odot$ the P continues to be sensitive to density distribution. Thus polarization measurements provide a better diagnostic tool to detect density and magnetic field variations in the corona. We show that Stokes profiles are sensitive to the velocity fields in the corona, thereby serving as diagnostic tools.

References

Casini, R. & Lin, H. 2002, *ApJ*, 571, 540
House, L. L. 1972, *Solar Phys*, 23, 103
Megha, A., Sampoorna, M., Nagendra. K. N., & Sankarasubramanian, K. 2017, *ApJ*, 841, 129
Saito, K. 1970, *Am Tokyo Astr. Obs., Ser.* 2,12, 53
Stenflo, J. O. 1994, *Solar Magnetic Fields* (Dordrecht: Kluwer)

https://doi.org/10.1017/S1743921318001023 Published online by Cambridge University Press